

Preparation of 3D-Porous Graphene Aerogel for High-Performance Anode of Lithium-Ion Batteries

Peng Li¹⁻³, Guiyun Yi^{1-4*}, Zhengting Zhang¹⁻³, Haiyang Fan¹⁻³, Yuanfeng Wu^{1-3*}, Weiwei Kang¹⁻³, Xiuxiu Zhang¹⁻³, Bing Xu¹⁻³, Yulong Zhang¹⁻³ and Qi Sun¹⁻³



¹College of Chemistry and Chemical Engineering, Henan Polytechnic University, China

²Collaborative Innovation Center of Coal Work Safety of Henan Province, China

³Henan Key Laboratory of Coal Green Conversion, Jiaozuo 454003, China

⁴State Collaborative Innovation Center of Coal Work Safety and Clean-efficiency Utilization, China

***Corresponding author:** Guiyun Yi, College of Chemistry and Chemical Engineering, Henan Polytechnic University, Henan Key Laboratory of Coal Green Conversion and State Collaborative Innovation Center of Coal Work Safety and Clean-efficiency Utilization, China

Yuanfeng Wu, College of Chemistry and Chemical Engineering, Henan Polytechnic University, Henan Key Laboratory of Coal Green Conversion, China

ARTICLE INFO

Received:  September 06, 2021

Published:  September 16, 2021

Citation: Peng Li, Guiyun Yi, Zhengting Zhang, Haiyang Fan, Yuanfeng Wu, et al., Preparation of 3D-Porous Graphene Aerogel for High-Performance Anode of Lithium-Ion Batteries. Biomed J Sci & Tech Res 38(5)-2021. BJSTR. MS.ID.006205.

ABSTRACT

Herein, a novel graphene aerogel (GA) with three dimensional (3D) porous structure was successfully prepared via a simple hydrothermal method, which was used as the anode active materials of lithium-ion batteries. Four samples with different hydrothermal reaction time (2 h, 6 h, 10 h, and 14 h) were comparably synthesized, and the electrochemical performance of all the synthesizes samples was measured. The porous electrode material was found to possess the highest specific capacity (113.8 mA h g⁻¹ at 2 A g⁻¹), the best rate capability and the most stable cycling performance (664.8 mA h g⁻¹ capacity retention at 100 mA g⁻¹ over 100 cycles). Such excellent electrochemical performance of the composite may be attributed to the rich porous and defective structure of graphene aerogels, which can offer more pathways for Li⁺ ions transportation and make the diffusion resistance decreasingly.

Keywords: Graphene Aerogel; Porous Electrode Material; Lithium-Ion Batteries; Anode Material

Introduction

Energy is recognized as an important material basis as well as a guarantee for human survival and development all the time [1,2]. However, with the excessive use of coal, petroleum and natural gas, the ever-increasing energy shortage and environmental contamination had become two major challenging problems facing all global nations. Thus, to effectively address such critical issues, extensive effort has recently been devoted to exploring efficient and clean energy conversion applications, such as lithium ion, sodium ion and fuel batteries. As an excellent energy storage device, lithium ion battery (LIBs) has attracted worldwide concerned and has

achieved commercialization. Due to the prestigious advantages of high power per unit mass, high cycle life and high safety performance, LIBs has been applied in a wide range of fields, such as in mobile phones, electric vehicles and aviation [3,4].

The structural configuration of LIBs mainly consists of positive and negative electrode materials, a diaphragm, electrolyte, and current collector [5]. In a typical discharging process, the Li⁺ generated by the negative electrode is embedded into the positive electrode through the electrolyte and the electrons are collected by the current collector and move in the opposite direction of the

external circuit [6]. While for charging, it is indeed the reverse process as described above. Thus, during the charging and discharging period, the more Li^+ ions moving between the positive and negative electrodes, the greater the activity being generated and the higher the charge-discharge specific capacity [7]. As a consequence, such principle of electrochemical conversion has confirmed that suitable anode materials are now playing pivotal role in improving electrochemical performance of LIBs.

As is well known, graphene, consisting of a single layer carbon atoms with sp^2 bonding, is a typically two-dimensional carbon material with outstanding excellent electrical conductivity and mechanical strength [8, 9]. Its theoretical capacity can reach up to 744 mAh g^{-1} , which is twice as much as that of graphite. This may be attributed to the fact that both sides of a graphene sheet can accommodate two Li^+ ions, in each hexagonal loop of carbon (Li_2C_6) [10]. Therefore, graphene is regarded as a potential candidate to substitute commercial graphite anodes and has been widely used in LIBs.

However, the powerful π - π stacking interactions and Van Der Waals forces lead to graphene sheets easily self-aggregate, which significantly reduces the available specific surface area and increases Li^+ ion transmission resistance [11]. In order to solve the aggregation problem, researchers have devised a great deal of advanced strategies. In particular, self-assembling graphene nanosheets into GA is one of the most effective methods. For example, our previous work demonstrated that PS nanospheres were used as sacrificial templates to fabricated nitrogen-rich graphene aerogel, where PS microsphere intercalation prevented the accumulation of layers in the GO sheet [12]. The obtained GA exhibited excellent electrochemical performance due to the layered porous structure. In addition, Zhang [13] et al. successfully fabricated free-standing nitrogen-doped graphene aerogel as the anode material for sodium ion batteries and it showed a high cycling performance ($287.9 \text{ mA h g}^{-1}$ after 200 cycles at a current density of 100 mA g^{-1}). In another similar work, Albarqouni [14] et al. successfully prepared rGO aerogel as supercapacitor electrode materials by utilizing the reduction capability of carbonic acid in soft drinks and enhanced charge storage capacity (121 F g^{-1} at 0.4 A g^{-1}). Thus, GA exhibit promising applications in electrochemistry field. However, to the best of our knowledge, works related to GA for LIBs are still limited.

In this work, GA used as the anode of LIBs were prepared by a facile hydrothermal strategy without any additives and templates. GA prevented the restacking of graphene nanosheets to enlarge the contact area between the electrolyte and the electrode, which simultaneously reduced ion and electron diffusion resistance [15]. Besides, it was feasible to tailor the oxygen-containing

functional group and surface defects of GA through adjusting the hydrothermal synthesis time. Benefiting from their porous structure and large specific surface area, the prepared GA-based LIBs show outstanding cycling stability (664.8 mAh g^{-1} at 0.1 A g^{-1} after 100 cycles) and superior rate capability, which demonstrates their potential application for Li^+ storage. The current research provides a valuable guidance for developing high-performance anode material for application in LIBs.

Experimental

Materials and Chemicals

All reagents were purchased commercially without further purification. GO was obtained by the method mentioned in our previously reported work [16].

Materials Characterization

To investigate the microstructure and morphology of the as-prepared samples, they are examined by advanced characterization tools like X-ray diffraction (XRD, Bruker, Germany), ULTRA 55 scanning electron microscope (SEM, ZEISS, Germany) and Raman spectroscopy (LabRAM HR 800 UV), respectively. The functional groups and elemental analysis of all samples were evaluated by X-ray photoelectron spectra (XPS) on ESCALAB 250Xi (Thermo Scientific, USA).

Electrochemical Measurements

The mixture of active materials, carbon black and polyvinylidene fluoride (PVDF) (weight ratio = 8:1:1) was dissolved in N-methyl-2-pyrrolidinone (NMP) solvent to prepare working electrodes. The assembling of 2016 coin-type cells was similar to that of reported previously. Cyclic voltammetry (CV) curves were recorded by a Shanghai Chenhua CHI 760e electrochemistry workstation in the range from 3.0 V to 0.01 V at 0.2 mV s^{-1} . Furthermore, galvanostatic charge/discharge cycles were measured using a NEWARE CT-4008 battery testing system at a current density range from 0.05 to 2 A g^{-1} versus Li/Li^+ .

Results and Discussion

Structural Characterization

Fig. 1(a) presents the preparation and lithium storage process of the GA. Firstly, 10 mL of GO (3 mg mL^{-1}) was transferred to 25 mL stainless-steel autoclave and then was maintained $180 \text{ }^\circ\text{C}$ for 2, 6, 10, and 14 h. Subsequently, the GA were obtained by freeze-drying and labeled as GA-2, GA-6, GA-10 and GA-14, respectively. The excellent Li^+ storage performance of GA-X electrode was due to the porous and defective structure of graphene aerogels, which can provide more Li^+ ions pathways and reduce diffusion resistance. In the process of hydrothermal reduction of graphene oxide, oxygen-

containing functional groups and hydrogen bonds on the surface of graphene oxide promote cross-linking between the sheets, and the gaps are filled with water molecules [5,17]. As a result, the porous structure is preserved by a sublimation process in freeze drying.

Shown in Figure 1(b~k) are the SEM images of all samples in order to investigate their morphologies and microstructures.

Through low magnification (Figure 1(b, d, h and j)) and high magnification (Figure 1(c, e, i, and k)), all samples exhibit the typically hierarchical and interconnected framework structure consisting of twisted and cross-linked graphene nano-sheets, which can provide more channels for Li^+ ions transport and reduce electrons transport resistance, thereby enhancing the electrochemical performance of GA-X.

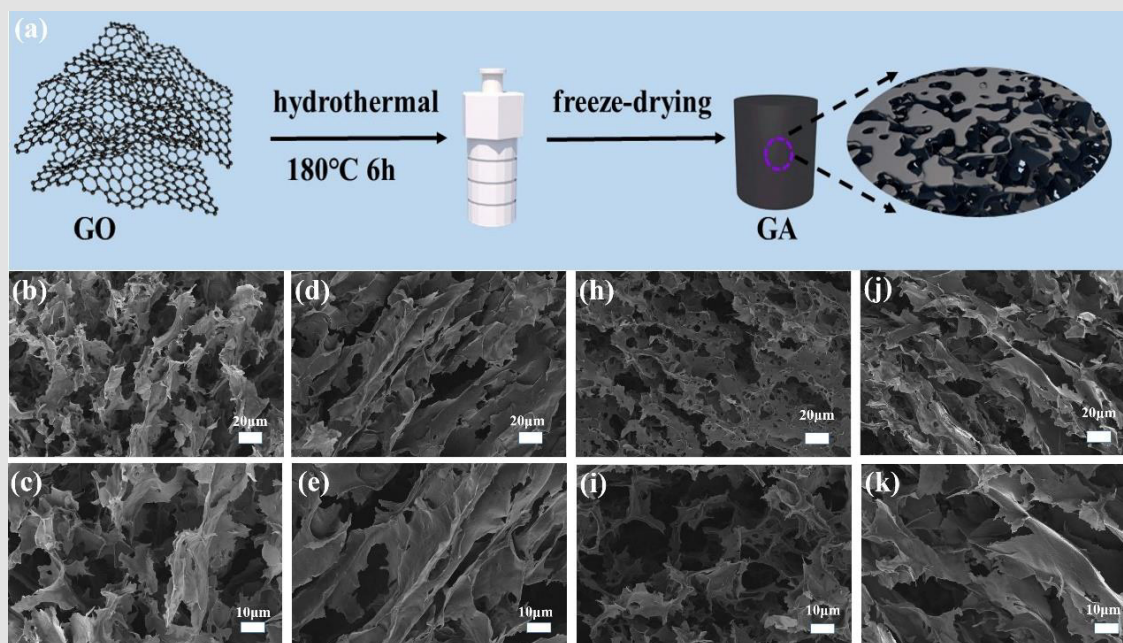


Figure 1: Schematic illustration of procedure to prepare GA anode and SEM images of GA-2(b, c), GA-6(d, e), GA-10(h,i) and GA-14(j,k).

To better clarify the structure variation of synthesized materials after the hydrogenation process, XRD, Raman and XPS measurements are performed. For comparison, Figure 2(a) shows the XRD patterns of graphite, GO, GA-2, GA-6, GA⁻¹⁰ and GA⁻¹⁴, respectively. It could be obviously observed that the characteristic peak of graphite appears at 26.3° , which corresponds to the interlamellar spacing of 0.348 nm [9,18]. After the Hummers method of oxidation process, the sharp peak shifted to 10.6° , which could be assigned to the (002) reflection [19], and the interlamellar spacing was expanded to 0.838 nm, which was caused by the presence of various oxygen-containing functional groups (hydroxyl, carboxyl, epoxy and carbonyl) and the introduction of H_2O molecules [20]. More importantly, after hydrothermal treatment, the broad (002) diffraction angle and interlayer spacing of GA-2, GA-6, GA⁻¹⁰ and GA⁻¹⁴ gradually increases to 24.48° (0.372 nm), 24.80° (0.367 nm), 24.94° (0.365 nm) and 25.14° (0.362 nm), respectively, which is attributed to the fact that the surface functional groups and intercalated H_2O molecules gradually decrease. This confirms that the hydrothermal time exerts different degrees of reduction impact on graphene oxide.

As can be seen from Raman spectra of all samples in Figure 2(b), two characteristic peaks at about 1348 and 1583 cm^{-1} appear [21]. G band represents the stretching vibration of sp^2 -bonded carbon atoms of graphitic layers, and D band corresponds to vibrations of sp^3 -bonded carbon atoms of the defective graphitic structure or disorders [22]. Generally, The D/G peak intensity ratio (ID/IG) value was used to assess the disorder of graphitic materials [23,24]. ID/IG of the GO (0.97), GA-2 (1.21), GA-6 (1.22), GA⁻¹⁰ (1.52) and GA⁻¹⁴ (1.61) increase with the increment of hydrothermal time, which was due to the partial removal of the oxygen-containing functional groups on the graphene surface, indicating the high degree of reduction in the process of crosslinking graphene into aerogels.

X-ray photoelectron spectroscopy (XPS), a significant characterization tool to give direct information about the elemental composition and surface functional groups of the obtained samples, has been carried out for further analysis. Two obvious peaks at 285 and 532 eV in Figure 2(c), which can be related to C and O elements, respectively [25]. More importantly, the atomic ratio of carbon and oxygen (C/O), is in the following order: GO (2.26) < GA-2 (4.52)

< GA-6 (4.76) ~ (GA⁻¹⁰ 4.73, GA⁻¹⁴ 4.71), which indicated that the oxygen functional groups of GA successfully are decomposed with the hydrothermal reaction time and no significant change occurs after six hours (the detailed data was shown in Table 1). Based on in-depth analysis of the shark peak in high resolution C 1s XPS spectrum (Figure 2d), four types of C species can be detected in those samples. Furthermore, the peaks located at 290.9, 288.3, 285.8 and 284.3 eV correspond to carboxyl groups (-COOR), carbonyl groups (C=O), epoxy groups (C-O), sp³ and sp² carbon, respectively [26-28]. Shown in Fig. 2(e) is the high resolution O1s spectra, from which it can be seen that GA exhibits four peaks at

the binding energy of 536.1, 532.8, 531.3 and 530.1 eV, which are assigned as the H₂O, HO-C=O, C-O-C and C=O, respectively [21, 29].

Table 1: Relative atomic percentages according to the XPS spectra.

Samples	C1s(%)	O1s(%)	Atomic ratio C/O
GO	69.3	30.7	2.26
GA-2	81.9	18.1	4.52
GA-6	82.6	17.4	4.76
GA-10	82.6	17.4	4.73
GA-14	82.5	17.5	4.71

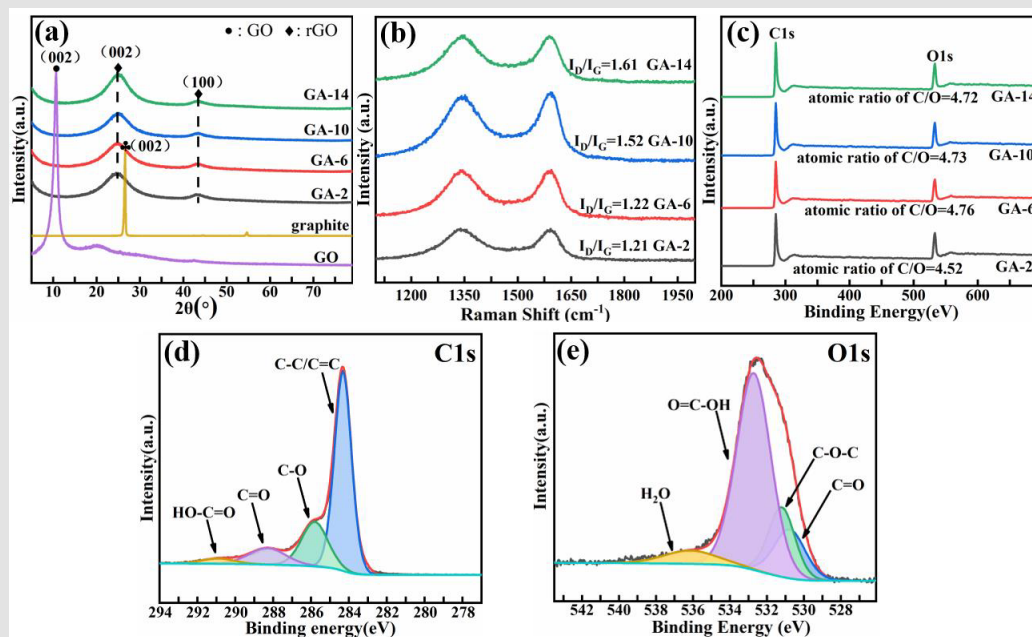


Figure 2: (a) XRD patterns; (b) Raman spectra; (c) XPS spectra of GA-X. High-resolution XPS spectra of (d) C 1s, and (e) O 1s in GA-6.

To further investigate the electrochemical properties of GA-X in LIBs, the corresponding samples are tested by the standard half-cell configuration. Shown in Figure 3(a) are the cyclic voltammogram curves (CVs) of the GA-6 electrodes with the first three cycles being measured at 0.2 mV s⁻¹. In the first cycle, a sharp reduction peak at 0.25 V appears, accounting for the irreversible decomposition of electrolyte and the subsequent formation of a solid electrolyte interface (SEI) film on the surface of carbonaceous structure [30-32]. In the subsequent cycles, CV curves are closely overlapped, which proves that the GA-6 anode has stable cyclic performance during the insertion and de-insertion process [33].

The charge-discharge curves of GA-6 composite materials in the 1st, 2nd, 3rd cycles are displayed in Figure 3(b). The GA-6 exhibits an initial charge and discharge capacity of 1744.4/976.8 mAh g⁻¹ and the Coulombic efficiency is 56.0% for LIBs, which far outweighs

that of others 1380.4/762.0 (55.2%), 1509.9/809.8 (53.6%), and 1411.8/828.1 (58.6%) mAh g⁻¹. The massive irreversible capacity loss for LIBs is caused by the SEI layer decomposition, irreversible reaction between Li⁺ and surface functional groups and irreversible desorption of ultra-fine pores [31]. Shown in Figure 3(c) are the testing results about the rate performance of GA-X anode at diversified current densities from 50 mA g⁻¹ to 2 A g⁻¹. In addition, the corresponding specific capacities of GA-6 are 671.2, 453.1, 292.9, 238.4, 201.2, 168.9 and 113.8 mAh g⁻¹, respectively, which can be observed in Figure 3(d). However, another three samples only exhibit specific capacities of 583.2, 384.3, 241.5, 188.4, 159.5, 133.8, and 89.7 mAh g⁻¹ for GA-2; 572.5, 387.6, 240.3, 194.1, 170.9, 143.8 and 91.3 mAh g⁻¹ for GA⁻¹⁰; 562.3, 366.8, 224.9, 187.8, 160.7, 133.8 and 83.8 mAh g⁻¹ for GA⁻¹⁴, respectively. It should be noted that when returning to the current condition of 100 mA g⁻¹, there is

still a reversible capacity of 428.4 mAh g⁻¹ in GA-6, higher than 355.8 (GA-2), 380.2 (GA⁻¹⁰) and 353.3 (GA⁻¹⁴) mAh g⁻¹. The dramatically enhanced Li⁺ storage capacity of GA-6 is mainly because the three-dimensionally porous structure is capable of providing more Li⁺ ion transport channels and electrical conductivity [34-36].

Shown in Figure 3(e) is the information on the cycling stabilities of the four samples, and the corresponding test was performed at 100 mA g⁻¹. As the hydrothermal reaction time increases, GA-6 (about 664.8 mAh g⁻¹) exhibits a significantly enhanced cycling performance than GA-2 (around 499.9 mAh g⁻¹) after 100 cycles. This may be ascribed to the reason that the hydrothermal time

is too short, which leads to insufficient reduction and too many oxygen-containing functional groups. When the hydrothermal time continues to increase, the capacity decays again (around 560.7 and 577.6 mAh g⁻¹) due to the excessive aging of graphene oxide. The results obviously indicates that the hydrothermal synthesis time exerts great impact on the electrochemical performance of the anode. Additionally, as shown in Figure 3(e), all GA anodes show nearly 100% coulombic efficiency, which further confirms that the cycling stability of the obtained GA materials is very high for LIBs (Figure 4).

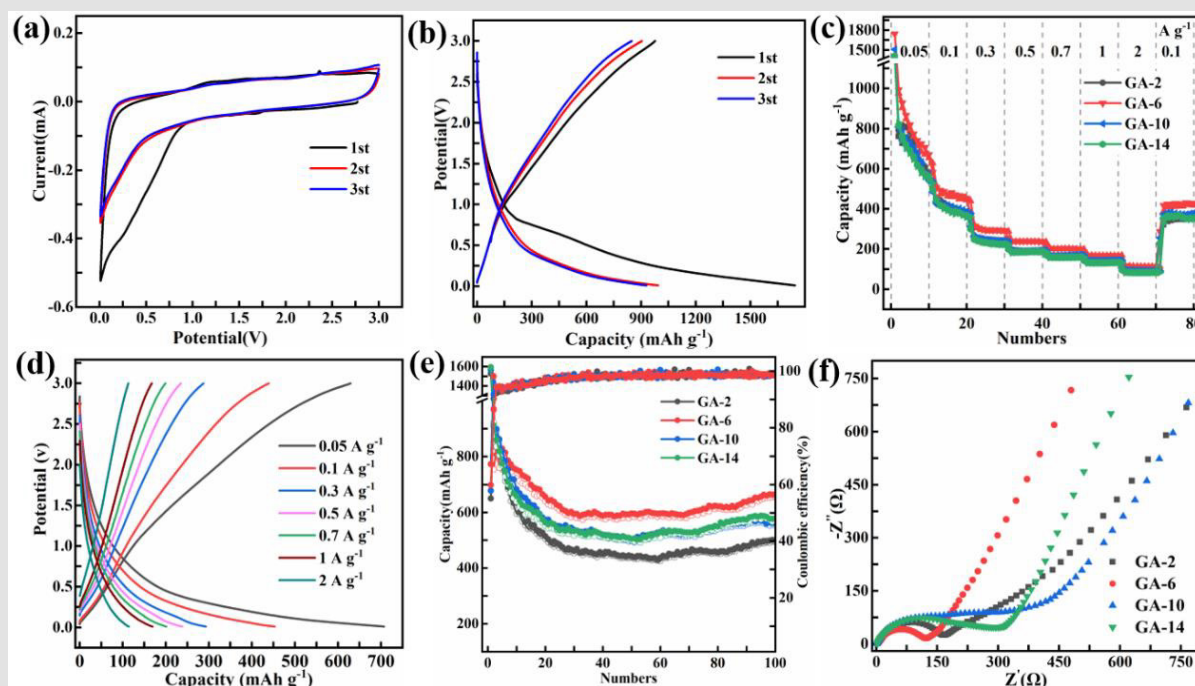


Figure 3: (a) CV curves of GA-6 at a scan rate of 0.2 mV s⁻¹. (b) Charging/discharging of GA-6 at current density of 50 mA g⁻¹. (c) Rate performances of GA-X electrodes. (d) The rate capabilities of GA-6 electrodes cycled at different current densities. (e) The cycling performance of GA-X electrodes in 100 cycles at 100mA g⁻¹. (f) Nyquist plots of the GA-X.

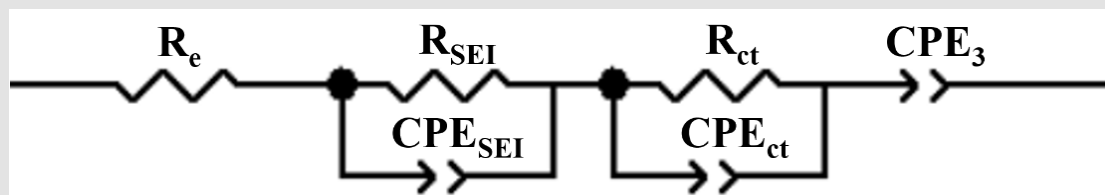


Figure 4: Nyquist plots of the electrodes.

The electrochemical impedance spectra (EIS) measurements are shown in Figure 3(f), which can further explain and verify the superior electrochemical performance. Nyquist plots of the composite illustrates an arc at the frequent regions corresponding to the interfacial charge-transfer resistance [37,38], and an

approximate straight sloping line at the less frequent regions corresponding to Warburg impedance [39]. By contrast, GA-6 has a smaller semicircle and a higher slope, which is attributed to the porous structure preventing the self-aggregation of the GO sheets and providing more Li⁺ ion diffusion channels. In addition, the GA-X

samples have the same equivalent circuit fitting values (Table 2) and the result affirms that the GA-6 composite possesses a smaller charge transfer impedance R_{SEI} (100.3 Ω) and R_{ct} (20.6 Ω) than the GA-2 (150.8 Ω and 38 Ω), GA-10 (225.1 Ω and 2.4 Ω) and GA-14 (135.7 Ω and 176.8 Ω), which demonstrated that porous structure could decrease charge-transfer resistance and improve the electrical conductivity. In addition, to better quantitatively analyze the testing data, an ideal equivalent circuit is utilized for fitting the impedance spectra, as is displayed in Figure 4. R_e denotes the resistance caused by the electrolyte, R_{SEI} represents the resistance of the electrode surface film, R_{ct} is the charge-transfer resistance and CPE_{SEI} and CPE_{ct} are constant phase elements assigned as the surface film and double layer capacitance, respectively, and CPE_3 is the constant phase element [40,41].

Table 2: The detailed values of the equivalent circuit components used for fitting the experimental curve.

Sample	R_e (Ω)	R_{SEI} (Ω)	R_{ct} (Ω)
GA-2	3.7	150.8	2.8
GA-6	1.9	100.3	20.6
GA-10	3	225.1	2.4
GA-14	2.7	135.7	176.8

Conclusions

In summary, a simple yet effective hydrothermal approach was reported to synthesize self-assembled porous carbon framework (GA) with prestigious advantages of large surface area, specific porous structure, superior electronic conductivity, excellent mechanical characteristic and ultrafast electron transport kinetic. Benefiting from their surface defects and abundant porosity, the 3D porous graphene exhibits highly stable cycling performance (664.8 mAh g^{-1} at 0.1 A g^{-1} after one hundred cycles). Moreover, it is convinced that by controlling the hydrothermal synthesis time, the surface defects of GA can be easily tailored. Correspondingly, GA-6 obtained by hydrothermal reaction for GA-6 exhibits the highest electrochemical performance. The present work provides a simple strategy to the design of electrodes with high performance for LIBs.

Acknowledgements

This work was supported by the National Key Research Plan (2018YFB0604500), the National Natural Science Foundation of China (U1803114), the Key Scientific and Technological Project of Henan Province (202102210183), the China Postdoctoral Science Foundation (207500), Outstanding Foreign Scientists Studio of Coal Green Conversion of Henan Province (GZS2020012), National Natural Science Foundation of China (51974110) and the Program for Science & Technology Innovation Talents in Universities of Henan Province (21HASTIT008).

References

- Zhao H, Xing B, Zhang C, Huang G, Yu J, et al. (2020) MnOX-modified corrugated carton-derived hierarchical porous carbon with ultrafast kinetics behaviour for high-performance symmetric supercapacitors. *Journal of Alloys and Compounds* 848: 156423.
- Zhao H, Xing B, Zhang C, Huang G, Liu Q, et al. (2018) Efficient synthesis of nitrogen and oxygen co-doped hierarchical porous carbons derived from soybean meal for high-performance supercapacitors. *Journal of Alloys and Compounds* 766: 705-715.
- Zhong Y, Wu P, Ge S, Wu Y, Shi B, et al. (2020) An egg holders-inspired structure design for large-volume-change anodes with long cycle life. *Journal of Alloys and Compounds* 816: 152497.
- Wu Q, Jiang R, Liu H (2020) Carbon layer encapsulated Fe_3O_4 @Reduced graphene oxide lithium battery anodes with long cycle performance. *Ceramics International* 46(8): 12732-12739.
- Fan X, Chen X, Dai L (2015) 3D graphene-based materials for energy storage. *Current Opinion in Colloid & Interface Science* 20(5-6): 429-438.
- Blomgren GE (2016) The development and future of lithium-ion batteries. *Journal of The Electrochemical Society* 164(1): A5019.
- Wu Y, Huang X, Huang L, Chen J (2021) Strategies for Rational Design of High-Power Lithium-ion Batteries. *Energy & Environmental Materials* 4(1): 19-45.
- Zhang L, Shi G (2011) Preparation of highly conductive graphene hydrogels for fabricating supercapacitors with high-rate capability. *The Journal of Physical Chemistry C* 115(34): 17206-17212.
- Chen X, Han J, Lv X, Lv W, Pan Z, et al. (2019) Dense yet highly ion permeable graphene electrodes obtained by capillary-drying of a holey graphene oxide assembly. *Journal of Materials Chemistry A* 7(20): 12691-12697.
- Chen K, Song S, Liu F, Xue D (2015) Structural design of graphene for use in electrochemical energy storage devices. *Chemical Society Reviews* 44(17): 6230-6257.
- Shao JJ, Lv W, Yang QH (2014) Graphene: Self-Assembly of Graphene Oxide at Interfaces (*Adv. Mater.* 32/2014). *Advanced Materials* 26(32): 5732-5732.
- Yi G, Li P, Xing B, Tian Q, Zhang X, et al. (2021) Nitrogen-rich graphene aerogel with interconnected thousand-layer pancake structure as anode for high performance of lithium-ion batteries. *Journal of Solid-State Chemistry* 294: 121859.
- Zhang J, Li C, Peng Z, Liu Y, Zhang J, et al. (2017) 3D free-standing nitrogen-doped reduced graphene oxide aerogel as anode material for sodium ion batteries with enhanced sodium storage. *Scientific reports* 7(1): 1-7.
- Albarqouni YM, Lee SP, Ali GA, Ethiraj AS, Algarni H, et al. (2021) Facile synthesis of reduced graphene oxide aerogel in soft drink as supercapacitor electrode. *Journal of Nanostructure in Chemistry* 1-11.
- Deng Y, Luo C, Zhang J, Qiu D, Cao T, et al. (2019) Fast three-dimensional assembly of MoS₂ inspired by the gelation of graphene oxide. *Science China Materials* 62(5): 745-750.
- Fan H, Yi G, Tian Q, Zhang X, Xing B, et al. (2020) Hydrothermal-template synthesis and electrochemical properties of Co₃O₄/nitrogen-doped hemisphere-porous graphene composites with 3D heterogeneous structure. *RSC Advances* 10(60): 36794-36805.
- Tao Y, Kong D, Zhang C, Lv W, Wang M, et al. (2014) Monolithic carbons with spheroidal and hierarchical pores produced by the linkage of functionalized graphene sheets. *Carbon* 69: 169-177.

18. Wang J, Shi Z, Fan J, Ge Y, Yin J, et al. (2012) Self-assembly of graphene into three-dimensional structures promoted by natural phenolic acids. *Journal of Materials Chemistry* 22(42): 22459-22466.
19. Liu LL, Zhang HJ, Li S, Yang C, Yang PX (2015) On the Chemical Reduced Large Specific Surface Area Graphene Oxide and its Electrochemical Performances. In *Applied Mechanics and Materials* 723: 615-618.
20. Islam MM, Subramaniyam CM, Akhter T, Faisal SN, Minett AI, et al. (2017) Three-dimensional cellular architecture of sulfur doped graphene: self-standing electrode for flexible supercapacitors, lithium ion and sodium ion batteries. *Journal of Materials Chemistry A* 5(11): 5290-5302.
21. Jiang Z, Zhang C, Qu X, Xing B, Huang G, et al. (2021) Humic acid resin-based amorphous porous carbon as high rate and cycle performance anode for sodium-ion batteries. *Electrochimica Acta* 372: 137850.
22. Xiao L, Wu D, Han S, Huang Y, Li S, et al. (2013) Self-assembled Fe₂O₃/graphene aerogel with high lithium storage performance. *ACS applied materials & interfaces* 5(9): 3764-3769.
23. Ferrari AC, Meyer JC, Scardaci V, Casiraghi C, Lazzeri M, et al. (2006) Raman spectrum of graphene and graphene layers. *Physical review letters* 97(18): 187401.
24. Li R, Li J, Qi K, Ge X, Zhang Q, et al. (2018) One-step synthesis of 3D sulfur/nitrogen dual-doped graphene supported nano silicon as anode for Li-ion batteries. *Applied Surface Science* 433: 367-373.
25. Tang F, Jiang T, Tan Y, Xu X, Zhou Y (2021) Preparation and electrochemical performance of silicon@ graphene aerogel composites for lithium-ion batteries. *Journal of Alloys and Compounds* 854: 157135.
26. Byon HR, Gallant BM, Lee SW, Shao-Horn Y (2013) Role of oxygen functional groups in carbon nanotube/graphene freestanding electrodes for high performance lithium batteries. *Advanced functional materials* 23(8): 1037-1045.
27. Hu C, Zhai X, Liu L, Zhao Y, Jiang L, et al. (2013) Spontaneous reduction and assembly of graphene oxide into three-dimensional graphene network on arbitrary conductive substrates. *Scientific reports* 3(1): 1-10.
28. Ye M, Dong Z, Hu C, Cheng H, Shao H, et al. (2014) Uniquely Arranged Graphene-on-Graphene Structure as a Binder-Free Anode for High-Performance Lithium-Ion Batteries. *Small* 10(24): 5035-5041.
29. Sahoo M, Sreena KP, Vinayan BP, Ramaprabhu S (2015) Green synthesis of boron doped graphene and its application as high-performance anode material in Li ion battery. *Materials Research Bulletin* 61: 383-390.
30. Kang W, Lin B, Jiang Z, Liu Z, Feng L, et al. (2019) Bi₂O₂CO₃ microspheres anchored on reduced graphene oxide nanosheets as electrode material for lithium-ion batteries and supercapacitors. *Materials Letter* 240: 299-302.
31. An SJ, Li J, Daniel C, Mohanty D, Nagpure S, et al. (2016) The state of understanding of the lithium-ion-battery graphite solid electrolyte interphase (SEI) and its relationship to formation cycling. *Carbon* 105: 52-76.
32. Han J, Kong D, Lv W, Tang DM, Han D, Zhang C, et al. (2018) Caging tin oxide in three-dimensional graphene networks for superior volumetric lithium storage. *Nature communications* 9(1): 1-9.
33. Zhang E, Jia X, Wang B, Wang J, Yu X, et al. (2020) Carbon dots@rGO paper as freestanding and flexible potassium-ion batteries anode. *Advanced Science* 7(15): 2000470.
34. Wang B, Ruan T, Chen Y, Jin F, Peng L, Zhou Y, et al. (2020) Graphene-based composites for electrochemical energy storage. *Energy storage materials* 24: 22-51.
35. Yu M, Zhang J, Li S, Meng Y, Liu J (2016) Three-dimensional nitrogen doped holey reduced graphene oxide framework as metal-free counter electrodes for high performance dye-sensitized solar cells. *Journal of Power Sources* 308: 44-51.
36. Wei W, Yang S, Zhou H, Lieberwirth I, Feng X, et al. (2013) 3D graphene foams cross-linked with pre-encapsulated Fe₃O₄ nanospheres for enhanced lithium storage. *Advanced materials* 25(21): 2909-2914.
37. Xing B, Zeng H, Huang G, Zhang C, Yuan R, et al. (2019) Porous graphene prepared from anthracite as high-performance anode materials for lithium-ion battery applications. *Journal of Alloys and Compounds* 779: 202-211.
38. Pei M, Wu Y, Qi Z, Mei D (2020) Synthesis and electrochemical performance of NiO/Fe₃O₄/rGO as anode material for lithium-ion battery. *Ionics* 26(8): 3831-3840.
39. Zeng H, Xing B, Zhang C, Chen L, Zhao H, et al. (2020) In situ synthesis of MnO₂/porous graphitic carbon composites as high-capacity anode materials for lithium-ion batteries. *Energy & Fuels* 34(2): 2480-2491.
40. Lv Q, Song R, Wang B, Zhu H, Xu J, et al. (2020) Three-dimensional nitrogen-doped graphene aerogel toward dendrite-free lithium-metal anode. *Ionics* 26(1): 13-22.
41. Tan C, Cao J, Khattak AM, Cai F, Jiang B, et al. (2014) High-performance tin oxide-nitrogen doped graphene aerogel hybrids as anode materials for lithium-ion batteries. *Journal of Power Sources* 270: 28-33.

ISSN: 2574-1241

DOI: 10.26717/BJSTR.2021.38.006205

Guiyun Yi, Yuanfeng Wu. Biomed J Sci & Tech Res



This work is licensed under Creative Commons Attribution 4.0 License

Submission Link: <https://biomedres.us/submit-manuscript.php>**Assets of Publishing with us**

- Global archiving of articles
- Immediate, unrestricted online access
- Rigorous Peer Review Process
- Authors Retain Copyrights
- Unique DOI for all articles

<https://biomedres.us/>